# CEBAF Program Advisory Committee Six (PAC6) Proposal Cover Sheet

This proposal must be received by close of business on April 5, 1993 at:

CEBAF
User Liaison Office
12000 Jefferson Avenue
Newport News, VA 23606

## Proposal Title

The $p(\vec{e},e'\vec{N})\pi$ Reaction with HARP

## Contact Person


**Name:** Prof. James J. Kelly
**Institution:** University of Maryland
**Address:** Department of Physics
**Address:** University of Maryland
**City, State ZIP/Country:** College Park, MD 20742
**Phone:** 301-405-6109 **FAX:** 301-314-9525
**E-Mail → BITnet:** KELLY@umdenp **Internet:** KELLY@enp.umd.edu


**If this proposal is based on a previously submitted proposal or letter-of-intent, give the number, title and date:**

**CEBAF Use Only**

Receipt Date: 4/5/93 Log Number Assigned: PR 93-013

By: JP

# The $p(\vec{e}, e'\vec{N})\pi$ Reaction with HARP

J.J. Kelly (spokesperson), H. Breuer, N.S. Chant, P. Markowitz,
T.M. Payerle, P.G. Roos
*University of Maryland, College Park, Maryland 20742, U.S.A.*

Th.S. Bauer, H.W. den Bok, H. Willering
*Rijksuniversiteit te Utrecht, 3508 TA Utrecht, Netherlands*

D.G. Ireland, G. van der Steenhoven
*NIKHEF-K, 1009 AJ, Amsterdam, Netherlands*

B.L. Berman, W.J. Briscoe, P.L. Cole, J.P. Connelly, K.S. Dhuga,
W.R. Dodge, Z. Papandreou, S.L. Rugari
*Center for Nuclear Studies, George Washington University,*
*Washington D.C. 20052, U.S.A.*

G.M. Huber, G.J. Lolos
*University of Regina, SK S4S OA2 Canada*

C. Furget, S. Kox, E. Voutier
*Institut de Sciences Nucléaires, F-38026 Grenoble, France*

R.W. Lourie
*University of Virginia, Charlottesville, VA 22901, U.S.A.*

J.M. Finn
*The College of William and Mary, Williamsburg, VA 23185, U.S.A.*

S. Nanda, P.E. Ulmer
*Continuous Electron Beam Facility, Newport News, VA 23606, U.S.A.*

April 2, 1993

## Abstract

We propose to begin a systematic exploration of the $p(\vec{e}, e'\vec{n})\pi^+$ and $p(\vec{e}, e'\vec{p})\pi^0$ reactions using the HARP detector by measuring selected in-plane and out-of-plane response functions for $W = 1.232$ and $W = 1.44$ GeV, corresponding to the peaks of the delta and Roper resonances. The measurements will be performed with $\epsilon = 0.9$ so that HARP can be placed at large enough angles to take advantage of its large converter. At $Q^2 = 0.5$ (GeV/c)$^2$ the large angular acceptance of HARP allows the entire angular distribution for pion electroproduction of the $\Delta$ to be sampled. The Roper measurements will be performed at $Q^2 = 0.23$ (GeV/c)$^2$ to complement some of the $p(\vec{e}, e'\vec{p})\pi^0$ measurements planned in proposal 91-11 and will cover an angular range of $\pm 40°$ in the center of mass. With HARP centered on **q**, angular distributions for $R_{TT}$, $R'_{TT}$, and $R^t_{LT}$ will be obtained from measurements made with the HARP converter in the vertical plane and angular distributions for $R_{LT}$, $R'^t_{LT}$, and $R'^t_{TT}$ will be obtained using the HARP converter in the horizontal plane. Additional measurements with HARP in the vertical plane but centered on floor angles greater that $\theta_q$ will provide slices through the opening-angle cone that can be used to determine other response functions through the azimuthal dependence of the reaction. These measurements also provide valuable internal consistency checks. In the $\Delta$ region many of the interference response functions are sensitive to the quadrupole deformation of the $N \rightarrow \Delta$ transition. In the Roper region, many of the response functions are quite sensitive to possible longitudinal excitation of the Roper resonance.


Requirements

| | |
|---|---|
| Beam energy | : 2.33 GeV |
| Beam current | : 100 $\mu A$ |
| Beam polarization | : >60% |
| Duty factor | : $\sim$ 80% |
| Target | : $LH_2$, 1.0 g/cm$^2$ |
| Detectors | : HRS1 and HARP |
| Beam time | : 984 hours |

# 1 INTRODUCTION

Given that coupling to the pion dominates the low-lying excitations of the nucleon, high-quality pion electroproduction data are crucial to testing models of baryon structure. However, the presence of many overlapping resonances makes the analysis of such data quite complicated and the extraction of specific multipole amplitudes difficult. Fortunately, interference between resonant and nonresonant amplitudes tends to amplify small contributions to the reaction mechanism, thereby enhancing the sensitivity to interesting aspects of baryon structure. For example, Lourie has shown that recoil polarization observables in the $p(\vec{e}, e'\vec{p})\pi^0$ reaction provide good sensitivity to the $E2/M1$ ratio in the $N \rightarrow \Delta$ transition [1] and to the longitudinal excitation of the Roper resonance [2]. Observation of interference amplitudes requires either target polarization, recoil polarization, out-of-plane (OOP) measurements, or some combination of these elements [3]. Since no single type of experiment suffices to permit complete multipole decomposition of the reaction amplitude to be performed, it will be necessary to perform experiments with at least two of the three elements listed above. Furthermore, each of the available charge states should be measured in order to decompose the isospin structure.

The quadrupole deformation of the $\Delta$, due to the color hyperfine interaction, is sensitive to the underlying quark wave function. However, the available data do not even determine the sign of this crucial quantity unambiguously. (See Refs. [4, 5] for a survey of those data.) Furthermore, current models also vary widely in their predictions. Hence, it is important to obtain a definitive measurement of the quadrupole deformation of the $N \rightarrow \Delta$ transition and many proposals have been submitted to several laboratories for that purpose. Unfortunately, a method free of substantial model dependence does not appear to exist. Therefore, it will be necessary to acquire high-quality data for several reactions and to attempt to describe all of the data consistently using sophisticated reaction models.

Similarly, although the $P_{11}(1434)$ (Roper) resonance has been clearly established in pion photoproduction, its contribution to electroproduction is much less certain. The Roper resonance is usually interpreted as a radial $1s \rightarrow 2s$ quark excitation, which would yield a substantial longitudinal response. There is some evidence for longitudinal enhancement of inclusive electron scattering near $W \sim 1.44$ GeV, but the data are sparse. Alternatively, there has been speculation that the Roper resonance could be a hybrid baryon of the form $(1s)^3g$ in which a valence gluon is present while all three quarks remain in the lowest orbital [6]. In that case the longitudinal response would be absent or highly suppressed, a possibility which is not excluded by the data presently available.

Lourie has demonstrated that recoil polarization measurements for $p(\vec{e}, e'\vec{p})\pi^0$ would be sensitive to longitudinal excitation of the Roper resonance and could distinguish between these models, but no polarization data exist in that region. Investigation of these issues using $HRS^2$ in Hall A is the subject of CEBAF proposal 91-11. However, measurement of the out-of-plane (OOP) response functions is dif-

ficult for spectrometer experiments, perhaps even prohibitively so, yet the OOP response functions also provide good sensitivity to differences between various models of the electromagnetic structure of baryons. In fact, we find that many of the OOP response functions for both the $p(\vec{e},e'\vec{p})\pi^0$ and $p(\vec{e},e'\vec{n})\pi^+$ reactions are even more sensitive to differences between various models of the Roper resonance than are the response functions accessible to spectrometer experiments. Analogous quantities can also be obtained using large-acceptance devices, such as CLAS, with polarized targets. However, such devices are usually limited to relatively low luminosities. Since different combinations of multipole amplitudes enter many of the response functions for target versus recoil polarization, a consistent analysis of both experiments should, in principle, permit separation of some of the contributions. The greater the number of independent response functions which are available, the more completely the multipole amplitudes can be untangled and the more stringently models can be tested.

We propose to begin a systematic exploration of the $p(\vec{e},e'\vec{n})\pi^+$ and $p(\vec{e},e'\vec{p})\pi^0$ reactions using the HARP detector by measuring selected in-plane and out-of-plane response functions for $W = 1.232$ and $W = 1.44$ GeV, corresponding to the peaks of the delta and Roper resonances. The HARP detector uses the asymmetry of the $p(N,p)N$ reaction to determine the polarization of the incident nucleon, where $N$ represents either a proton or a neutron. A charged-particle tagger differentiates between protons and neutrons so that, in principle, both experiments can be performed simultaneously. For nucleon angles large enough to permit HARP to be placed close to the target, the $\pm 40$ cm converter dimensions provide considerable out-of-plane range. The measurements will be performed with $\epsilon = 0.9$ so that HARP can be placed at large enough angles to take advantage of its large converter. At $Q^2 = 0.5$ $(\mathrm{GeV/c})^2$ the large angular acceptance of HARP allows the entire angular distribution for pion electroproduction of the $\Delta$ to be sampled. The Roper measurements will be performed at $Q^2 = 0.23$ $(\mathrm{GeV/c})^2$ to complement some of the $p(\vec{e},e'\vec{p})\pi^0$ measurements planned in proposal 91-11 and will cover an angular range of $\pm 40°$ in the center of mass. With HARP centered on $\mathbf{q}$, angular distributions for $R_{TT}$, $R'_{TT}$, and $R'_{LT}$ will be obtained from measurements made with the HARP converter in the vertical plane and angular distributions for $R_{LT}$, $R'_{LT}$, and $R'_{TT}$ will be obtained using the HARP converter in the horizontal plane. Additional measurements with HARP in the vertical plane but centered on floor angles greater that $\theta_q$ will provide slices through the opening-angle cone that can be used to determine other response functions through the azimuthal dependence of the reaction. These measurements also provide tests of the internal consistency of the measurents and of the systematic errors. The proposed measurements cover a larger angular range and include several response functions not available to proposal 91-11; the measurements in common to both experiments will provide valuable tests of the consistency between the two experiments.

We are also investigating the possibilities for rotation and/or lifting of HARP to further enhance its capabilities for out-of-plane measurements. Although we

anticipate embarking upon a systematic program of measurements which would include many of the possible OOP response functions over a wider kinematic range, this initial proposal focuses primarily upon the simpler response functions which can be obtained directly from measurements of the transverse components of the polarization of the recoil nucleon using both vertical and horizontal orientations of the converter with its central axis within the scattering plane.

In Sec. 2 we present calculations for several representative models which indicate the degree of sensitivity to interesting aspects of the physics expected for the various observables. In Sec. 3 we discuss the proposed measurements in detail. The kinematics, observables, and response functions for pion electroproduction are reviewed in an appendix, which also serves to establish our notation.

# 2 Models of Pion Electroproduction

In this section we use several of the available models of pion electroproduction to compare the sensitivities of the $p(\vec{e}, e'\vec{n})\pi^+$ and $p(\vec{e}, e'\vec{p})\pi^0$ reactions to several interesting aspects of baryon structure. Although each of these models can be criticized theoretically, they nevertheless can help to survey the experimental possibilities. Calculations directly applicable to the proposed measurements are presented in the following section.

A description of the kinematics, observables, and response functions for electroproduction experiments can be found in the appendix, which also serves to define our (almost standard) notation. Regrettably, no accepted standard for the signs and normalizations of the response functions has gained wide acceptance. The calculations shown here were performed using the program *EPIPROD*, which is based in part upon an earlier program by Lourie. However, Lourie's program contained several serious errors which are corrected in *EPIPROD*. Those errors affect the calculations in his $p(\vec{e}, e'\vec{p})\pi^0$ proposal and in Refs. [1, 2], but are more serious for the $p(\vec{e}, e'\vec{n})\pi^+$ reaction. Therefore, we often compare results for both reactions herein. Complete documentation for *EPIPROD*, which includes many options not described here, can be found in Ref. [7].

Selected Feynman diagrams for pion production by a virtual photon are illustrated in Fig. 1 for generic meson+baryon models. Resonances in the $s$-channel are portrayed by Fig. 1a, where the heavy horizontal line indicates an excited state with isospin $\frac{1}{2}$ ($N^*$) or $\frac{3}{2}$ ($\Delta$). The remaining diagrams represent various non-resonant contributions, which are often called "Born terms". Diagrams b, c, and d of Fig. 1 contribute in both pseudoscalar and pseudovector coupling of the $\pi$NN system. Diagram e is the point contact or "seagull" term and is present only in the case of pseudovector coupling, where it is needed to restore gauge invariance. Diagram f depicts the exchange of an $\omega^0$ or a $\rho^0$, which does not contribute to charged pion production but may prove to be significant in the neutral pion production amplitude.

Excitation functions for the cross section and induced polarization of the $p(e, e'\vec{n})\pi^+$ and $p(e, e'\vec{p})\pi^0$ reactions in parallel kinematics with $Q^2 = 0.25$ (GeV/c)$^2$ and fixed $\epsilon$ are shown in the nucleon-resonance region in Fig. 2. These calculations employ the Devenish and Lyth parametrization of the resonances [8, 9, 10] and the von Gehlen representation of the nonresonant amplitudes [11], and are designated DLvG. The Devenish and Lyth model uses fixed-$t$ dispersion relations to parametrize the amplitudes for the $P_{33}(1232)$ ($\Delta$), $P_{11}(1434)$ (Roper), $D_{13}(1520)$, $S_{11}(1535)$, $S_{31}(1630)$, $S_{11}(1700)$, $D_{15}(1675)$, $F_{15}(1680)$, $F_{37}(1950)$, and $G_{17}(2190)$ resonances. The von Gehlen parametrization uses pseudoscalar coupling to describe the nonresonant amplitudes for the $\pi NN$ system. The dominance of the $\Delta$ resonance is clearly evident, whereas the Roper resonance is particularly notable for its obscurity. Higher resonances give the excitation function structure, but no single resonance stands out for $W > 1.4$ GeV.

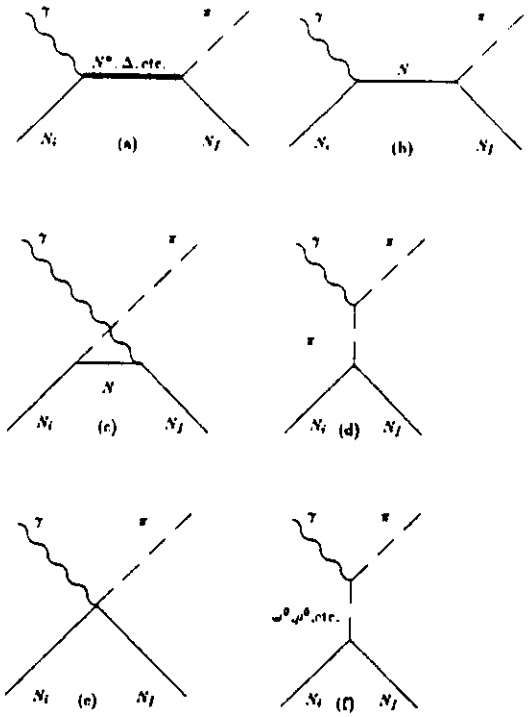

Figure 1: Feynman diagrams for pion production. (a) is the resonant diagram($s$-channel), (b) and (c) nucleon $s$-pole and $u$-pole terms, (d) is the pion $u$-pole term, (e) is the point-contact("seagull") term, and (f) is the heavy meson $u$-pole term, including $\omega^0$, $\rho^0$, etc.

## 2.1 Delta Excitation

The sensitivity of the nucleon polarization to the $E2/M1$ ratio is illustrated in Fig. 3, which compares calculations for parallel kinematics using the nominal values of $E2/M1 = 2\%$ and $C2/M1 = 5\%$ with calculations which either omit or invert the sign of the quadrupole deformation. Interference endows polarization with much more sensitivity to the quadrupole contribution than the cross section. We find that the neutron (proton) polarization is substantially enhanced (reduced) by inversion of the quadrupole deformation. The fact that variations of the quadrupole amplitude have opposite effects on the neutron and proton polarizations can be exploited as a sensitive test of the internal consistency of any model used to extract the quadrupole amplitude from the polarization data. Furthermore, possible observation of a small value for the polarization would still convey much information.

To illustrate the sensitivity to the quadrupole deformation the $\Delta$ expected for angular distributions of the response functions we propose to measure , we compare in Fig. 4 selected LT response functions and in Fig. 5 selected TT response functions for $W = 1.232$ GeV and $Q^2 = 0.5$ (GeV/c)$^2$ for both reactions. Dotted curves use

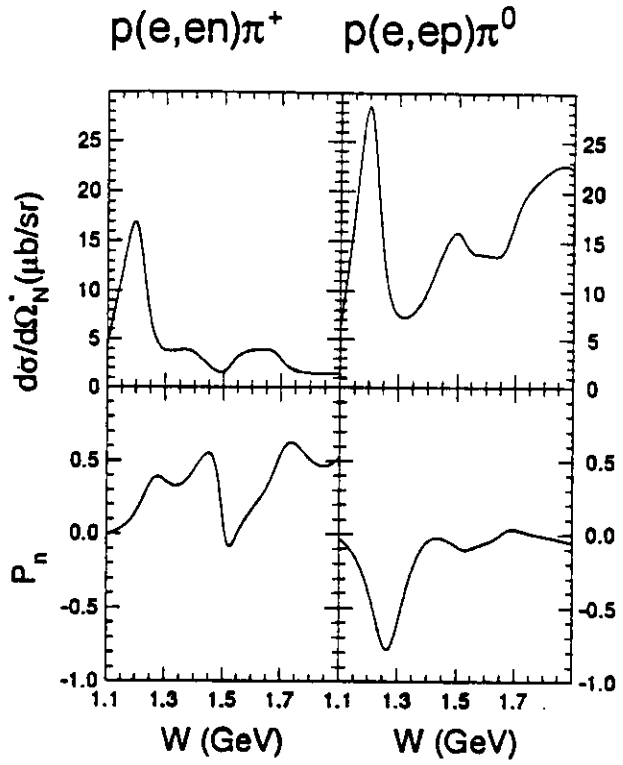


Figure 2: Excitation functions for the cross section and induced polarization in parallel kinematics for the $p(e,e'\vec{n})\pi^+$ and $p(e,e'\vec{p})\pi^0$ reactions using $Q^2 = 0.25$ (GeV/c)$^2$ and $\epsilon = 0.9$. The calculations are based upon the DLvG model.

the DLvG parameters, dot-dashed curves omit the quadrupole deformation, and the solid curves invert the sign of the quadrupole deformation. Both reactions show good sensitivity to this quantity, with the effects in each response function being significantly different for the two reactions. The sensitivity of the longitudinal-transverse interference response functions to the quadrupole amplitude is particularly impressive. The proposed measurements will obtain angular distributions for all three LT response functions displayed in Fig. 4.

On the other hand, the predicted value of $P_n$ depends upon the model chosen. The inevitability of this model dependence can be justified by the following argument. The induced polarization depends upon the imaginary part of $E_{1+}^* M_{1+}$. According to the Fermi-Watson theorem [12], the scattering amplitudes for a resonance are characterized by a common phase, such that the imaginary part of an interference amplitude of this type vanishes for an isolated resonance. Therefore, a nonvanishing polarization requires interference between resonant amplitudes and either nonresonant amplitudes or underlying tails of other resonances. The latter cannot be specified unambiguously.

In Fig. 6 we show calculations for the $\Delta$ region using the model of Mehrotra and Wright (MW) [13], which is a generalization of the Blomqvist-Laget model (BL)

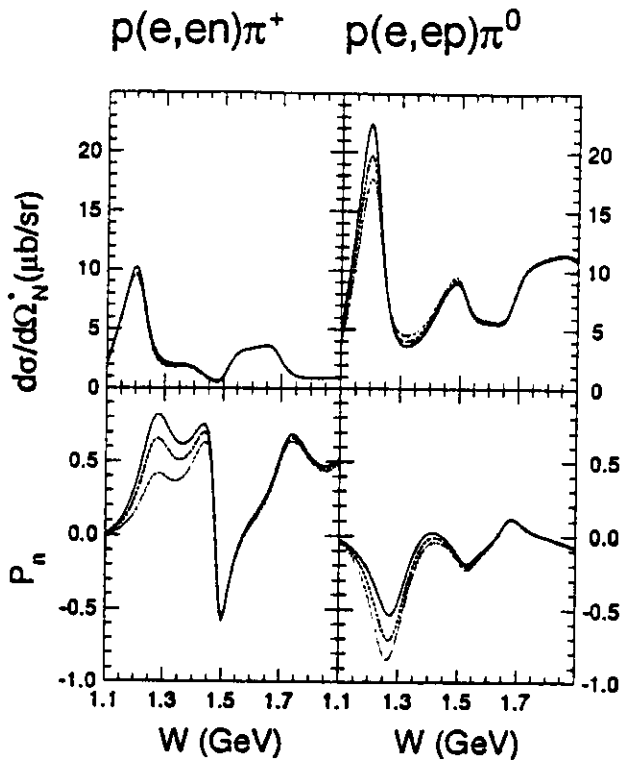


Figure 3: Sensitivity to the quadrupole deformation of the $\Delta$. Dotted curves use the DLvG parameters, whereas dot-dashed curves omit and solid curves invert the sign of the quadrupole deformation. Parallel kinematics with $Q^2 = 0.5$ (GeV/c)$^2$ and $\epsilon = 0.9$ were employed.

[14] to electroproduction. Unlike the DLvG model, the MW model employs pseudovector coupling and includes $\omega$ exchange and the $\Delta$ u-pole, but is nonrelativistic. Fortunately, the MW polarizations are relatively insensitive to differences among several fits to the pion form factor. However, the MW model does not include the quadrupole amplitude for the $N \rightarrow \Delta$ transition nor the effects of higher resonances. We find that with the MW model a large neutron polarization is predicted, considerably larger than found with the DLvG model, and that the proton polarization is much smaller than with the DLvG model.

One important difference between the DLvG and MW models appears to be the absence of quadrupole deformation in the MW model. However, the dotted and dash-dotted curves in Fig. 6 demonstrate that appreciable differences between the MW and DLvG models remain even after the quadrupole amplitude and the contributions of higher resonances are omitted from the DLvG model. Similarly, although $P_n$ for $p(e, e'\vec{n})\pi^+$ with $\theta^*_N \sim 0°$ is sensitive to the neutron electric form factor and to the pion form factor, whereas the $p(e, e'\vec{p})\pi^0$ reaction is not, the differences between those form factors are not sufficient to explain the differences between calculations based on these models. The large difference which remains for the proton polar-

ization, in particular, may be due to the $\omega$ $u$-pole, which is included in the MW model but not in the DLvG model. Hence, the requirement that a model must reproduce both polarizations simultaneously provides a stringent consistency check for the extraction of the $E2/M1$ ratio from polarization data.

Further differences between these models can be seen in the response functions shown in Figs. 7 and 8. Although both of these models were calibrated against data, several lacunae probably permit appreciable differences to remain. First, most of the data used to calibrate these models were obtained by observing the pion near the direction of the momentum transfer, corresponding to $\theta_N^* \sim 180°$. Second, most of the data were for photoproduction rather than electroproduction and hence are insensitive to the $LT$ response functions. Third, very few polarization data are available for electroproduction reactions.

The most complete model of pion electroproduction in the delta region presently available is the hamiltonian model of Nozawa, Blankleider, and Lee [15, 16, 17]. The electromagnetic matrix elements are deduced from Feynman amplitudes based upon a lagrangian that includes $\gamma$, $\pi$, $\rho$, $\omega$, N, and $\Delta$ fields. The $\pi N$ final-state interactions are based upon a separable potential which fits the pion scattering data below 500 MeV well. The model has been shown to be unitary and gauge invariant. We hope to be able to compare our experimental results with their calculations, but the DLvG model should suffice for estimates of count rates.

Therefore, the proposed experiment will supply some of the data needed to determine the inelastic response functions in the $\theta_N^* \sim 0°$ region where little information currently exists, especially for polarization quantities. These data will be sensitive to differences between various models of pion electroproduction and to the parameters of the $\Delta$ resonance.

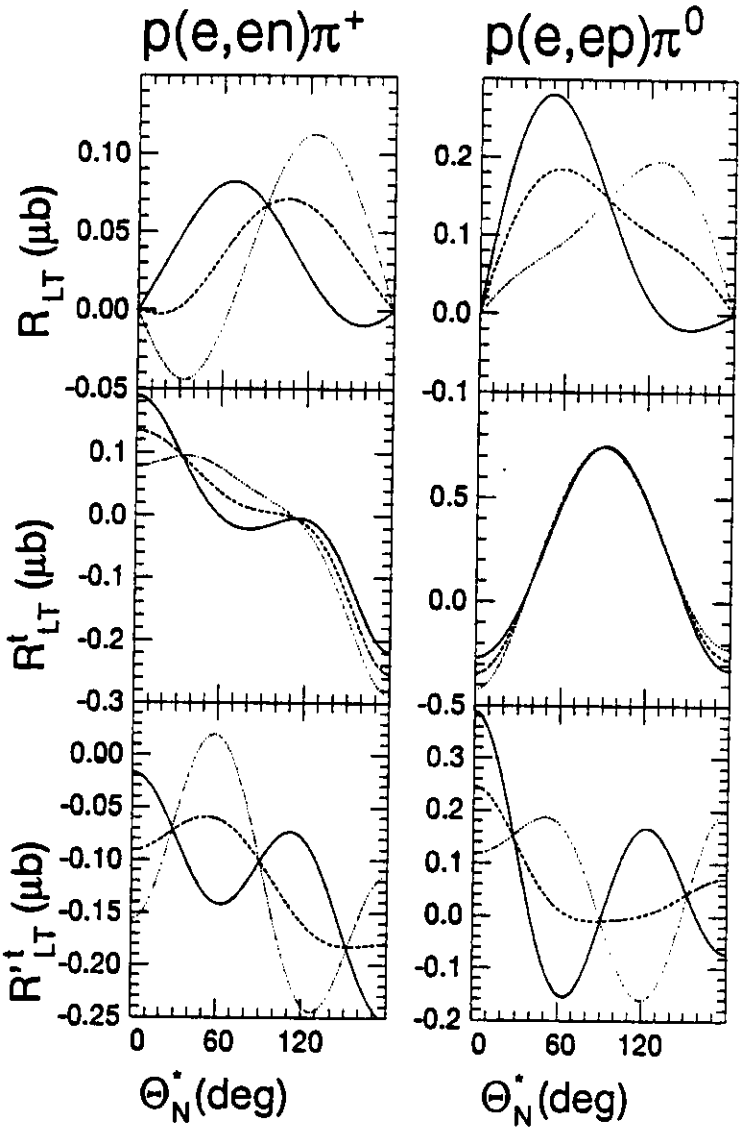


Figure 4: Angular distributions for selected LT response functions for $W = 1.232$ GeV and $Q^2 = 0.5$ (GeV/c)$^2$ are compared for the $p(\vec{e}, e'\vec{n})\pi^+$ and $p(\vec{e}, e'\vec{p})\pi^0$ reactions. Dotted curves use the DLvG parameters, whereas dot-dashed (solid) curves omit (invert) the quadrupole deformation. The calculations are based on the DLvG model.

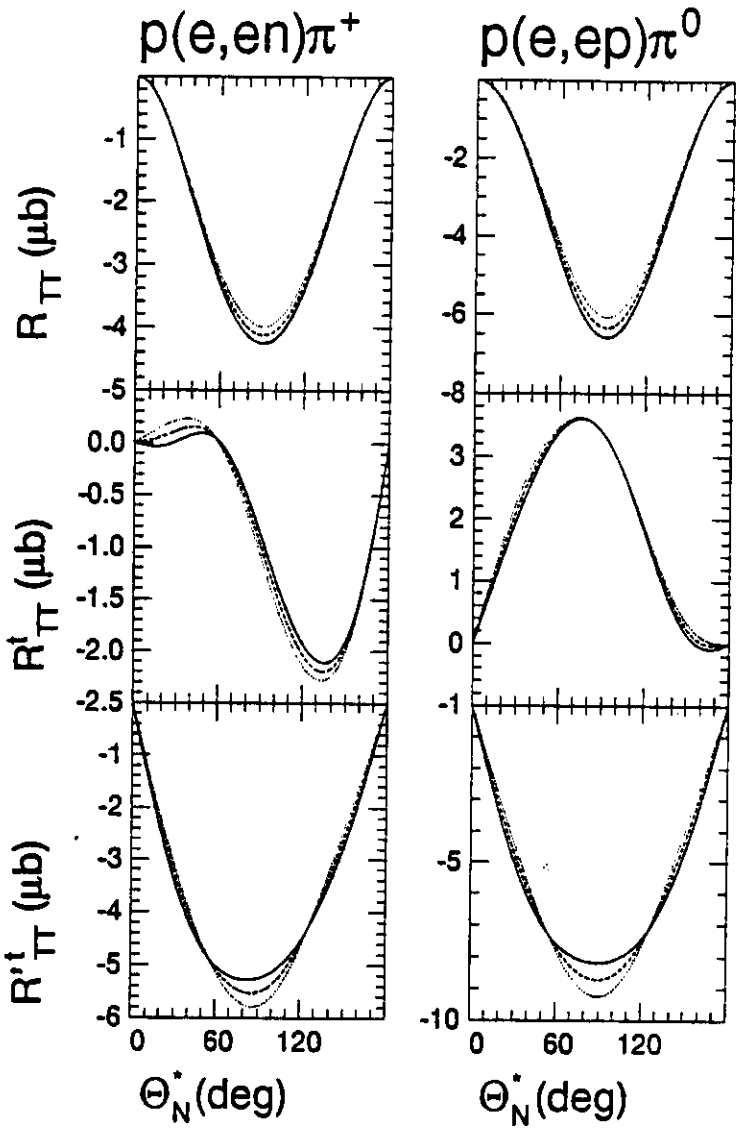


Figure 5: Angular distributions for selected TT response functions for $W = 1.232$ GeV and $Q^2 = 0.5$ (GeV/c)$^2$ are compared for the $p(\vec{e}, e'\vec{n})\pi^+$ and $p(\vec{e}, e'\vec{p})\pi^0$ reactions. Dotted curves use the DLvG parameters, whereas dot-dashed (solid) curves omit (invert) the quadrupole deformation. The calculations are based on the DLvG model.

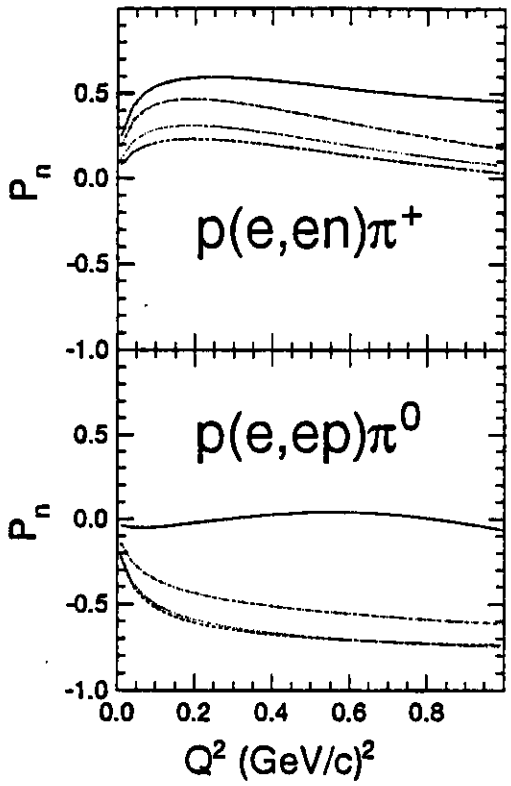


Figure 6: Model dependence of induced polarization near $\Delta$ resonance. Dashed curves are based upon the DLvG model and solid curves upon the MW model. In addition, the dotted curves omit all resonances above the $\Delta$ and the dash-dotted curves omit the quadrupole amplitude for the $\Delta$ in the DLvG model as well. Parallel kinematics with W = 1.232 GeV and $\epsilon = 0.9$ were employed.

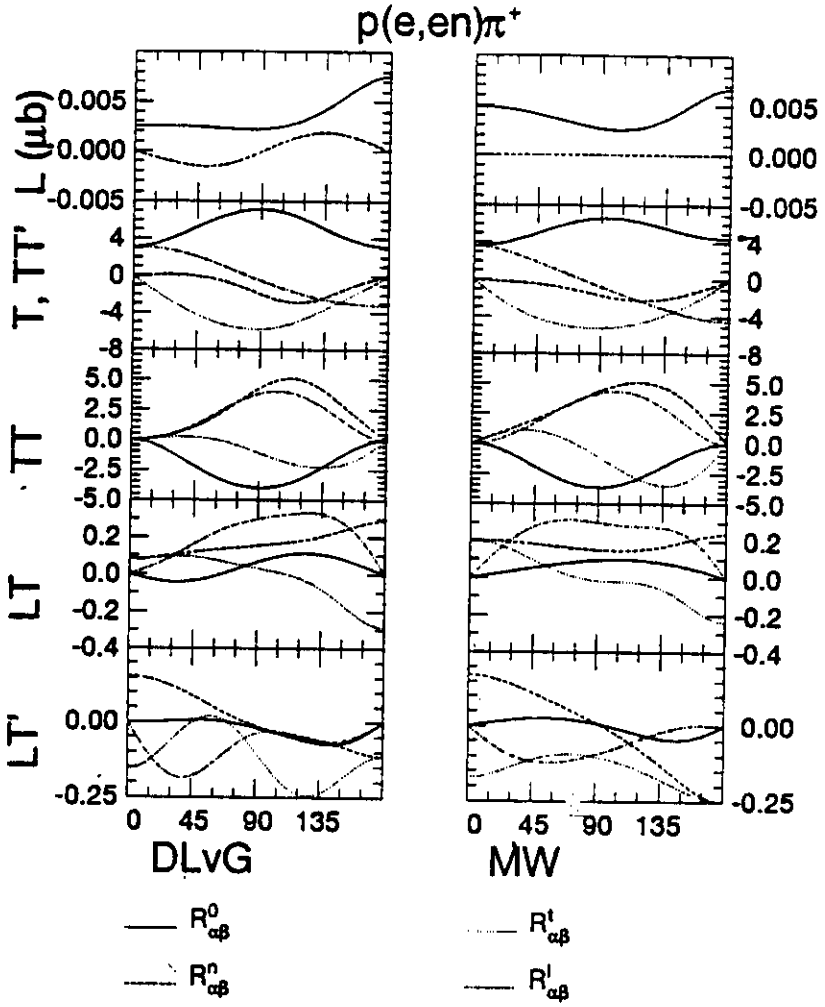


Figure 7: Response functions for the $p(\vec{e}, e'\vec{n})\pi^+$ reaction at $W = 1.232$ GeV and $Q^2 = 0.5$ (GeV/c)$^2$ are compared for the DLvG and MW models.

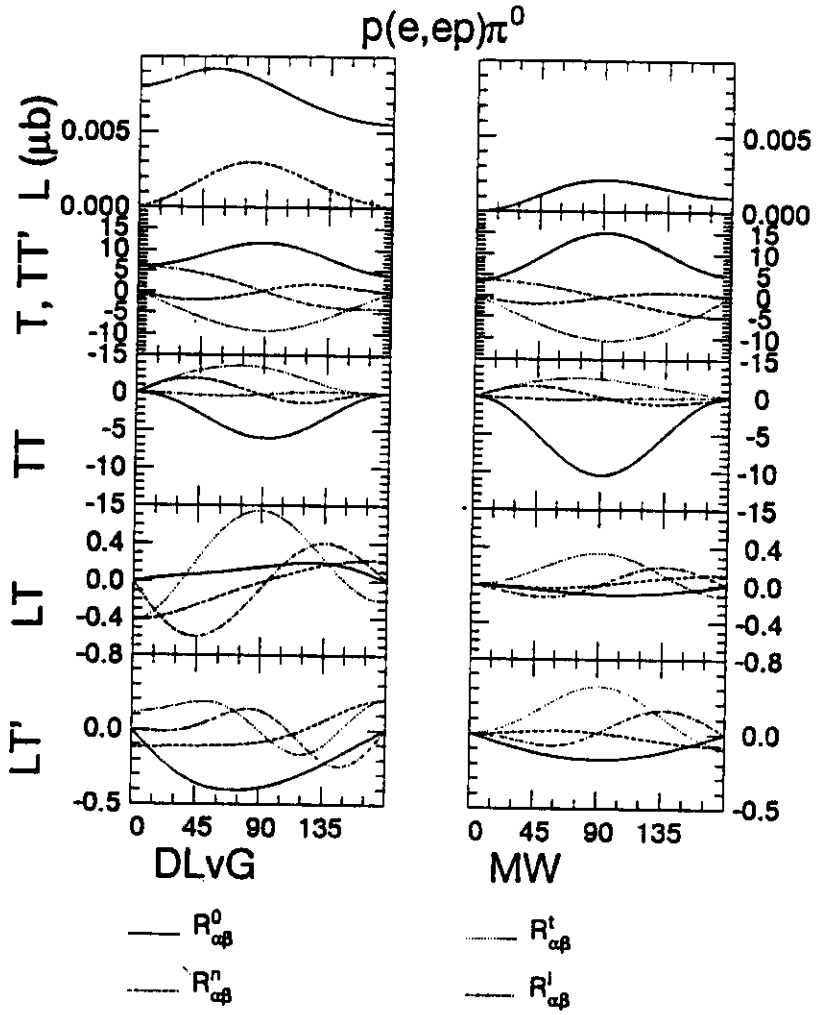


Figure 8: Response functions for the $p(\vec{e}, e'\vec{p})\pi^0$ reaction at $W = 1.232$ GeV and $Q^2 = 0.5$ (GeV/c)$^2$ are compared for the DLvG and MW models.

## 2.2 Roper Excitation

For the present purposes it suffices to examine the sensitivity of the various response functions to three assumptions for the structure of the Roper resonance. In Fig. 9 we compare helicity amplitudes for the radial excitation model with those for a hybrid baryon model in which the scalar amplitude vanishes [6]. For the third model, we assume that the Roper is absent altogether. To illustrate the sensitivity of the proposed measurements to the differences between these models, angular distributions for selected response functions for both the $p(\vec{e}, e'\vec{n})\pi^+$ and $p(\vec{e}, e'\vec{p})\pi^0$ reactions at $W = 1.44$ GeV and $Q^2 = 0.23$ (GeV/c)$^2$ are compared in Figs. 10 and 11 using these three models. Dotted curves omit the Roper, dot-dashed curves employ the hybrid baryon model, and solid curves assume radial excitation. The sensitivity to differences between these models appears to be generally greater for the $p(\vec{e}, e'\vec{n})\pi^+$ than for the $p(\vec{e}, e'\vec{p})\pi^0$ reaction.

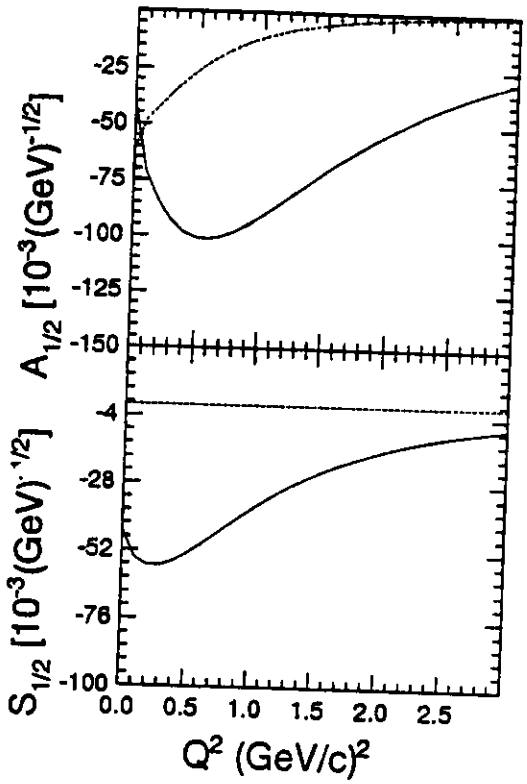


Figure 9: Helicity amplitudes for the Roper resonance. Dashed curves are based upon the hybrid baryon and the solid curve upon the radial excitation model.

Most of the response functions are similar when we assume either no Roper is present or that the Roper resonance is a hybrid baryon. Apparently, the transverse response is fairly small compared with other transverse contributions so that relatively precise measurements would be required to detect a dominantly transverse Roper excitation. However, the $R^t_{TT}$ response function for the $p(\vec{e}, e'\vec{n})\pi^+$ reaction

appears to differentiate clearly between transverse and no Roper excitation. Separation of that response function requires examination of the azimuthal dependence of the reaction, as provided by the proposed vertical slices through the opening-angle distribution. Conversely, the radial excitation model predicts strong effects upon the $R_{LT}^{t}$ response functions and should be relatively easy to confirm or refute. Significant sensitivity for the $p(\vec{e}, e'\vec{n})\pi^+$ reaction is also predicted in $R_{LT'}^{t}$, which in parallel kinematics is directly proportional to $\Pi_t$ and hence can be obtained in-plane. The most sensitive quantity for the $p(\vec{e}, e'\vec{p})\pi^0$ reaction appears to be $R_{LT'}^{n}$, which can be obtained in-plane but requires a left-right asymmetry and is not shown. Some of the response functions show greater relative differences at larger $Q^2$, but since the cross section is smaller measurements at higher $Q^2$ will be deferred to future proposals.

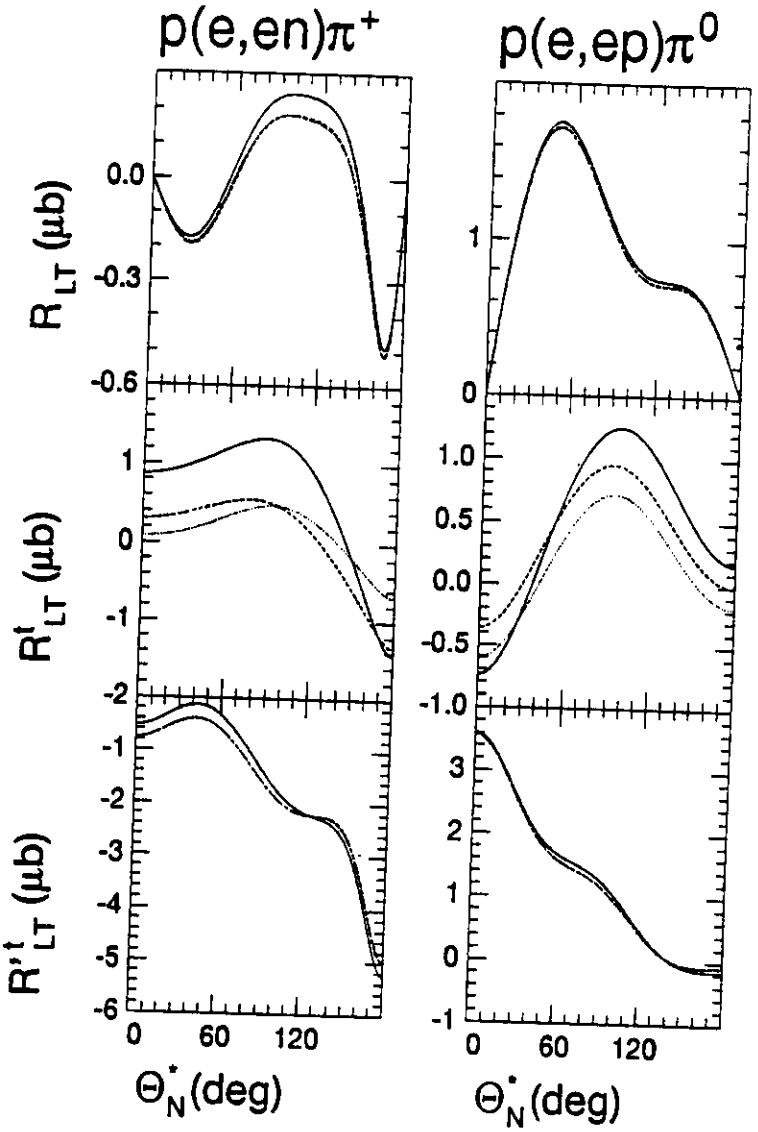


Figure 10: Angular distributions for selected LT response functions are compared for Roper excitation at $W = 1.44$ GeV and $Q^2 = 0.23$ (GeV/c)$^2$ for both the $p(\vec{e}, e'\vec{n})\pi^+$ and $p(\vec{e}, e'\vec{p})\pi^0$ reactions. Dotted curves omit the Roper resonance, dashed curves use the hybrid model, and solid curves assume radial excitation.

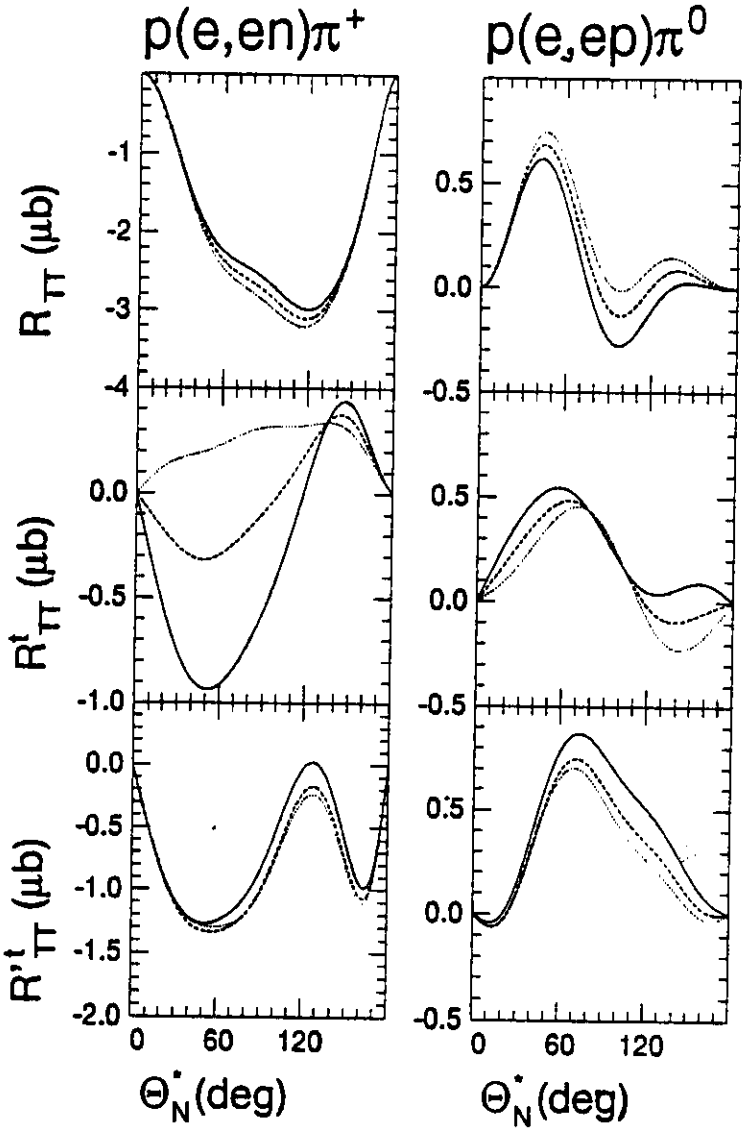


Figure 11: Angular distributions for selected TT response functions are compared for Roper excitation at $W = 1.44$ GeV and $Q^2 = 0.23$ (GeV/c)$^2$ for both the $p(\vec{e}, e'\vec{n})\pi^+$ and $p(\vec{e}, e'\vec{p})\pi^0$ reactions. Dotted curves omit the Roper resonance, dashed curves use the hybrid model, and solid curves assume radial excitation.

# 3 Experimental Program

## 3.1 The HARP Detector

A conceptual diagram of the HARP detector is given in Fig. 12. An incident nucleon scatters from protons in the liquid hydrogen converter and a recoil proton is detected. The energy of the recoil proton is determined by thick $E$-scintillators and its angle by wire chambers. The relationship between the recoil kinetic energy $T$ at angle $\theta$ to the incident energy $T_0$ is given by

$$T = \frac{2m_p T_0 \cos^2\theta}{2m_p + T_0 \sin^2\theta}.$$

Thin $\Delta E$-detectors are used for particle identification. The polarization of the incident nucleon is determined from the asymmetry of the conversion reaction.

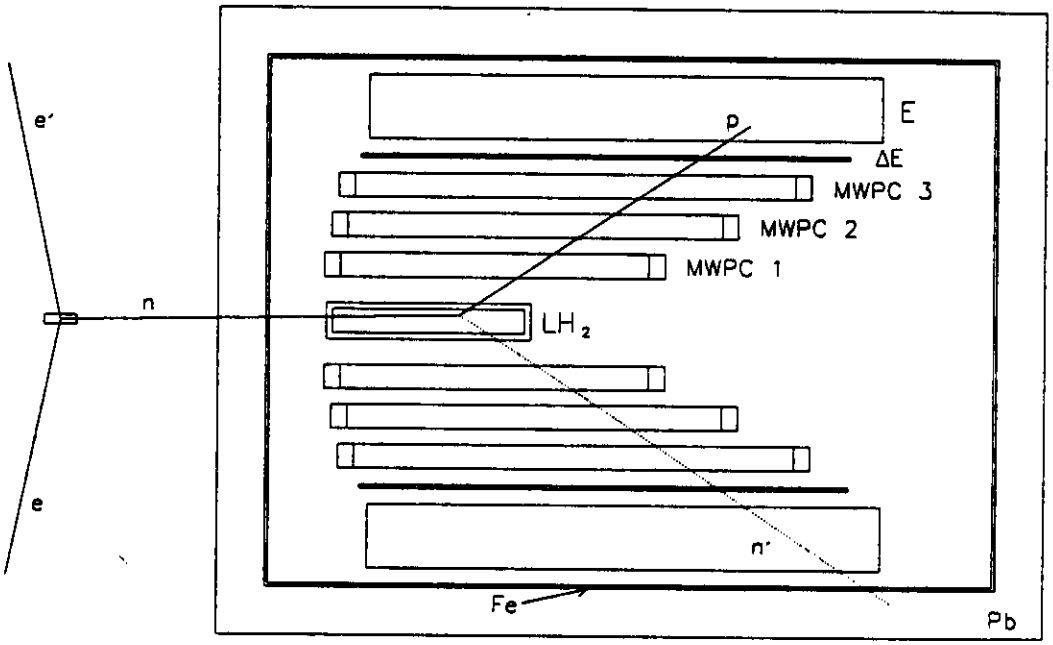


Figure 12: Conceptual diagram of HARP.

Recoil polarimetry has several advantages over time-of-flight (TOF) detectors. First, by employing an elementary analyzing reaction, calibration of the effective analyzing power for a complex material is not necessary. The dependence of the latter upon operating conditions makes reliable calibration difficult. Second, use of a passive converter in place of a TOF detector endows recoil polarimetry with

greater rate capability and better background suppression. Therefore, the figure-of-merit (FOM) is typically an order of magnitude better for HARP than for TOF polarimeters. On the other, the energy resolution of recoil polarimetry is limited by the intrinsic properties of the detector and cannot be significantly improved by simply increasing the flight path as for TOF detection. Therefore, the energy resolution for HARP is limited to about 10%. This limitation is not too serious for the present application, but does restrict the apparatus to experiments upon few-body systems.

For high energies the requirement that the recoil proton be stopped by the E-bars restricts the recoil angle to large values. Fortunately, the analyzing power also tends to be greatest at large angles. Simulations demonstrate that both the efficiency and figure of merit for neutron detection are approximately constant for energies above 200 MeV, where the efficiency is about 1% when the recoil angle is restricted to ensure that protons are stopped. The efficiency for proton detection is similar, but the figure of merit increases significantly with energy.

A segmented charged-particle detector before the converter will allow the scattering angle to be determined more accurately for protons than for neutrons. The individual tagger elements will be approximately $3 \times 3$ cm$^2$ and thus define a solid angle which can be compared for protons with the track reconstruction within HARP. Suppose that HARP is oriented with its converter vertical. Since the converter has a length of $\pm$ 40 cm, considerable out-of-plane (OOP) acceptance is available for scattering angles sufficiently large to permit HARP to be placed close to the target. For central scattering angles larger than 40°, the dimensions of the shielding enclosure permit HARP to placed at a converter distance of 80 cm from the target, such that angles as large as $\pm$26° out of plane can be reached. With an in-plane acceptance of 3 cm and with a nearly symmetrical acceptance for parallel kinematics being defined by the electron spectrometer, the natural solid angle bin matches the tagger dimensions of $3 \times 3$ cm$^2$, corresponding to about 1.4 msr per bin at a distance of 80 cm.

Let $\theta$ represent the laboratory opening angle for a cone centered upon q and let $\phi$ represent the azimuthal angle. The center of mass opening angle $\theta^*$ is larger, such that for given W and large enough $Q^2$ the entire $\theta^*$ distribution fits within the $\theta$ acceptance. Let $\theta_{nq}$ represent the floor angle between the converter and q where, by convention, positive $\theta_{nq}$ and $\phi = 180°$ corresponds to ejectile angles larger than $\theta_q$. Increasing $\theta_{nq}$ makes available larger $\theta$ values and varies $\phi$ according to the intersection of the $\theta$ cone with the converter. However, if the converter is maintained in the vertical orientation, the polarization it measures is a mixture of $\Pi_n$ and $\Pi_t$. Let the $\hat{x}$ axis be parallel to the floor, the $\hat{z}$ axis coincide with the nucleon momentum, and the $\hat{y}$ axis be within a vertical plane and given by $\hat{y} = \hat{z} \otimes \hat{x}$. The $\hat{t}$ and $\hat{n}$ axes are then related to the $\hat{x}$ and $\hat{y}$ axes by a rotation around the $\hat{l} = \hat{z}$ axis through an angle $\chi$, where

$$\tan \chi = \cos \theta \tan \phi.$$

When the converter is vertical, the left-right asymmetry in HARP is proportional

to $\Pi_y$; with converter horizontal, the up-down asymmetry gives $\Pi_x$.

The relationships between the polarization observables that HARP measures in its intrinsic coordinate system and the response functions specified in the Appendix are given below.

$$\begin{aligned}
\sigma_0 P_x &= \nu_{LT}(R^t_{LT}\sin\phi\cos\chi - R^n_{LT}\cos\phi\sin\chi) && (1)\\
&+ \nu_{TT}(R^t_{TT}\sin 2\phi\cos\chi - R^n_{TT}\cos 2\phi\sin\chi) && (2)\\
&- (\nu_L R^n_L + \nu_T R^n_T)\sin\chi && (3)\\
\sigma_0 P_y &= \nu_{LT}(R^t_{LT}\sin\phi\sin\chi + R^n_{LT}\cos\phi\cos\chi) && (4)\\
&+ \nu_{TT}(R^t_{TT}\sin 2\phi\sin\chi + R^n_{TT}\cos 2\phi\cos\chi) && (5)\\
&+ (\nu_L R^n_L + \nu_T R^n_T)\cos\chi && (6)\\
\sigma_0 P'_x &= \nu'_{LT}(R'^t_{LT}\cos\phi\cos\chi - R'^n_{LT}\sin\phi\sin\chi) + \nu'_{TT}R'^t_{TT}\cos\chi && (7)\\
\sigma_0 P'_y &= \nu'_{LT}(R'^t_{LT}\cos\phi\sin\chi + R'^n_{LT}\sin\phi\cos\chi) + \nu'_{TT}R'^t_{TT}\sin\chi && (8)
\end{aligned}$$

For the special case of $\phi = \chi = \pm 90°$, we obtain

$$\begin{aligned}
\sigma_0 &= \nu_L R_L + \nu_T R_T - \nu_{TT} R_{TT} && (9)\\
\sigma_0 P_x &= \pm(\nu_{TT} R^n_{TT} - \nu_L R^n_L - \nu_T R^n_T) && (10)\\
\sigma_0 P_y &= \nu_{LT} R^t_{LT} && (11)\\
\sigma_0 P'_x &= -\nu'_{LT} R'^n_{LT} && (12)\\
\sigma_0 P'_y &= \pm\nu'_{TT} R'^t_{TT}, && (13)
\end{aligned}$$

which permits the angular dependencies of $R^t_{LT}$ and $R'^t_{TT}$ to be isolated using the converter in the vertical orientation and $\theta_{nq} = 0$. In conjunction with measurements in the horizontal configuration, the azimuthal dependence of the cross section can be used to separate $R_{TT}$ from the combination $(\nu_L R_L + \nu_T R_T)$; of course, Rosenbluth separation of the latter requires variation of $\epsilon$ also. In principle, this configuration also permits $R'_{LT}$ to be extracted from the beam analyzing power, but most model calculations predict unpromisingly small values for that quantity.

Similarly, for the special case of $\phi = 0$ or $180°$, we obtain

$$\begin{aligned}
\sigma_0 &= \nu_L R_L + \nu_T R_T + \nu_{TT} R_{TT} \pm \nu_{LT} R_{LT} && (14)\\
\sigma_0 P_x &= 0 && (15)\\
\sigma_0 P'_y &= 0 && (16)\\
\sigma_0 P_y &= \nu_{LT} R^n_{LT} \pm (\nu_{TT} R^n_{TT} + \nu_L R^n_L + \nu_T R^n_T) && (17)\\
\sigma_0 P'_x &= \nu'_{LT} R'^t_{LT} \pm \nu'_{TT} R'^t_{TT}, && (18)
\end{aligned}$$

which permits the angular dependencies of $R_{LT}$, $R'^t_{LT}$, and $R''^t_{TT}$ to be obtained using the converter in the horizontal orientation and exploiting the left-right asymmetry of the cross section and of $P'_x$. The fact that $R''^t_{TT}$ can be obtained from polarization measurements at $\theta_{nq} = 0$ using the converter in either horizontal or vertical configurations provides an important test of the internal consistency and systematic

errors for polarization measurements. Furthermore, with the converter in the vertical configuration, measurements of $P_y$ in the scattering plane with $\theta_{nq}$ on opposite sides of q can be used to isolate $R^n_{LT}$. However, this technique can only be applied when $\theta_q$ is sufficiently large to allow HARP to be placed forward of q and will not be attempted in the present experiment.

For parallel kinematics ($\theta^*_N = 0$) it is useful to observe that azimuthal symmetry requires $R^t_{LT} = R^n_{LT}$, $R'^n_{LT} = -R'^t_{LT}$, and $R'^t_{TT} = 0$, such that

$$\sigma_0 = \nu_L R_L + \nu_T R_T \tag{19}$$

$$\sigma_0 P_x = 0 \tag{20}$$

$$\sigma_0 P'_y = 0 \tag{21}$$

$$\sigma_0 P_y = \nu_{LT} R^n_{LT} = \nu_{LT} R^t_{LT} \tag{22}$$

$$\sigma_0 P'_x = \nu'_{LT} R'^t_{LT} = -\nu'_{LT} R'^n_{LT}. \tag{23}$$

Finally, if the converter is oriented vertically and placed at an angle $\theta_{nq}$ with respect to q, each $\theta$ bin is obtained with a different $\phi$. If the nucleon passes through the converter at a height $y$, the opening and azimuthal angles are determined by

$$\tan\theta = \left[(\frac{y}{d})^2 + \tan^2\theta_{nq}\right]^{1/2} \tag{24}$$

$$\sin\phi = \pm\left[1 + (\frac{d}{y})^2 \tan^2\theta_{nq}\right]^{-1/2} \tag{25}$$

$$= \pm\left[1 - \frac{\tan^2\theta_{nq}}{\tan^2\theta}\right]^{1/2}. \tag{26}$$

Hence, in conjunction with the information obtained from the measurements described above, the $\phi$ dependence of $P_y$ and $P'_y$ can be used to at least partially separate $R^n_{LT}$, $R'^n_{LT}$, $R^t_{TT}$, $R'^n_{TT}$, and $(\nu_L R^n_L + \nu_T R^n_T)$. Thus, several vertical slices through the opening angle cone provide considerable sensitivity to the azimuthal dependence of the reaction. Also note that increasing $\theta_{nq}$ increases the angular range accessible to $R^t_{LT}$ and $R'^t_{TT}$.

Therefore, cross section measurements at $\theta_{nq} = 0$ with both horizontal and vertical configurations provide angular distributions for the $R_{LT}$ and $R_{TT}$ response functions. Simultaneous polarization measurments provide angular distributions for the $R^t_{LT}$, $R'^t_{LT}$, and $R'^t_{TT}$ response functions, for which no previous data presently exist. Additional measurements in the vertical configuration at several angles $\theta_{nq}$ with respect to q extend the angular range for $R^t_{LT}$ and $R^t_{TT}$ and provide information on $\phi$ dependences which can be used to disentangle several other response functions. Furthermore, with HARP both charged channels can be obtained simultaneously.

## 3.2 Proposed Measurements

Systematic exploration of the many polarized and OOP response functions for pion electroproduction of nucleon resonances obviously requires an extensive experimen-

tal program. However, to begin such an enterprise using a new detector at a new facility, it behooves us to focus upon an initial set of measurements which promise to yield interesting physics by exploiting the unique capabilities of the instrument while placing relatively modest demands upon the new facilities. More ambitious proposals exploiting the full OOP capabilities of the polarimeter will be submitted upon successful commissioning of the apparatus. We are also exploring the possibilities for rotation of the converter plane and/or lifting the entire detector out of plane. The former has the advantage of simplifying the relationships between detector coordinates and the reaction plane. The latter has the advantage of extending the OOP range, particularly when small $\theta_q$ requires large converter distances.

Therefore, we propose to measure the vertical and horizontal polarizations in the $p(\vec{e},e'\vec{n})\pi^+$ and $p(\vec{e},e'\vec{p})\pi^0$ reactions using both parallel and nonparallel kinematics. Initially we plan to perform measurements at $W = 1.232$ and 1.44 GeV, corresponding to the peaks of the $\Delta$ and Roper resonances, but expect to perform measurements at other invariant masses later. Some of the data for the $p(\vec{e},e'\vec{p})\pi^0$ reaction can be compared with the similar results anticipated for proposal 91-11. Since large OOP coverage requires small converter distances and hence large $\theta_q$, we have chosen to perform the measurements at $\epsilon = 0.9$, but may consider additional measurements at small $\epsilon$ later for the purposes of Rosenbluth analysis. For the $\Delta$ resonance we have chosen a value of $Q^2 = 0.5$ (GeV/c)$^2$, which is sufficiently large to compress the entire $\theta^*$ angular distribution onto the HARP converter. The smaller cross sections at the Roper resonance favor small $Q^2$ but the larger invariant mass favors large $Q^2$. For the Roper resonance we have chosen $Q^2 = 0.23$ (GeV/c)$^2$ to match the first $Q^2$ for proposal 91-11. Details of the kinematics may be found in Table 1. Some transverse kinematics with $\epsilon = 0.5$ are given for future reference but measurements are not proposed for those kinematics at this time. The maximum laboratory opening angle for each reaction is given as $\theta_{max}$.

Table 1: *Kinematics for $p(\vec{e},e'\vec{n})\pi^+$ at the $\Delta$ and Roper Resonances*

| W (GeV) | $Q^2$ (GeV/c)$^2$ | $\epsilon$ | $E_i$ (GeV) | $E_f$ (GeV) | $\theta_e$ (deg) | $\theta_q$ (deg) | $T_n$ (GeV) | $\theta_{max}$ (deg) |
|---|---|---|---|---|---|---|---|---|
| 1.232 | 0.5 | 0.9 | 2.333 | 1.727 | 20.29 | 40.01 | 0.443 | 18.5 |
| | | 0.5 | 1.110 | 0.504 | 56.46 | 26.78 | | |
| 1.44 | 0.23 | 0.9 | 2.335 | 1.577 | 14.36 | 25.83 | 0.509 | 42.5 |
| | | 0.5 | 1.156 | 0.398 | 41.40 | 17.05 | | |

Since HARP subtends the entire reaction cone for the chosen delta kinematics, we plan to cover the azimuthal distribution in 5 steps within the range $0 \leq \theta_{nq} \leq 18°$. However, at a laboratory angle of 26°, HARP cannot be placed closer to the target than about 1.6 m, where it subtends a laboratory angle of about $\pm 15°$, corresponding to a cone of $\pm 40°$ in the center of mass for the chosen Roper kinematics. Although

larger values of $\theta_N^*$ can be reached using $\theta_{nq} > 15°$, the $\phi$ distribution is then limited. Therefore, in order to maximize the azimuthal completeness of the measurements, we have decided to cover the $\theta_N^* \leq \pm 40°$ cone in 5 slices for the Roper kinematics also and to forego larger opening angles.

To illustrate the sensitivity of the proposed measurements to the quadrupole deformation the $\Delta$, we compare calculations of center of mass cross sections and laboratory polarization components using the converter in the vertical and horizontal orientations in Figs. 13 and Figs. 14, respectively, where $W = 1.232$ GeV, $Q^2 = 0.5$ (GeV/c)$^2$, and $\epsilon = 0.9$. Dotted curves used the DLvG parameters, dot-dashed curves omit the quadrupole deformation, and the solid curves invert the sign of the quadrupole deformation. In the vertical orientation, the transverse polarization observables for both reactions show good sensitivity to the quadrupole amplitude, as was also evident in $P_n$ for parallel kinematics. In the horizontal orientation, the substantial left-right asymmetry is sensitive to the $R_{LT}$ response function and through that to the quadrupole amplitude. Also note that the proposed noncentral slices through the reaction cone will provide sensitivity to $R_{TT}$ and give the transverse polarization components additional degrees of freedom and variability, but the corresponding angular distributions are too numerous to display here.

To illustrate the sensitivity of the proposed measurements to longitudinal excitation of the Roper resonance, we compare calculations of center of mass cross sections and laboratory polarization components using the converter in the vertical and horizontal orientations in Figs. 15 and Figs. 16, respectively, where $W = 1.44$ GeV, $Q^2 = 0.23$ (GeV/c)$^2$, and $\epsilon = 0.9$. Dotted curves omit the Roper, dot-dashed curves employ the hybrid baryon model, and solid curves assume radial excitation. Measurement of the transverse polarization observables for the $p(\vec{e}, e'\vec{n})\pi^+$ reaction could easily distinguish radial excitation of the Roper resonance in either configuration and in the vertical configuration can also detect a hybrid Roper. Additional information and sensitivity to the differences between various models will also be provided by noncentral slices through the reaction cone.

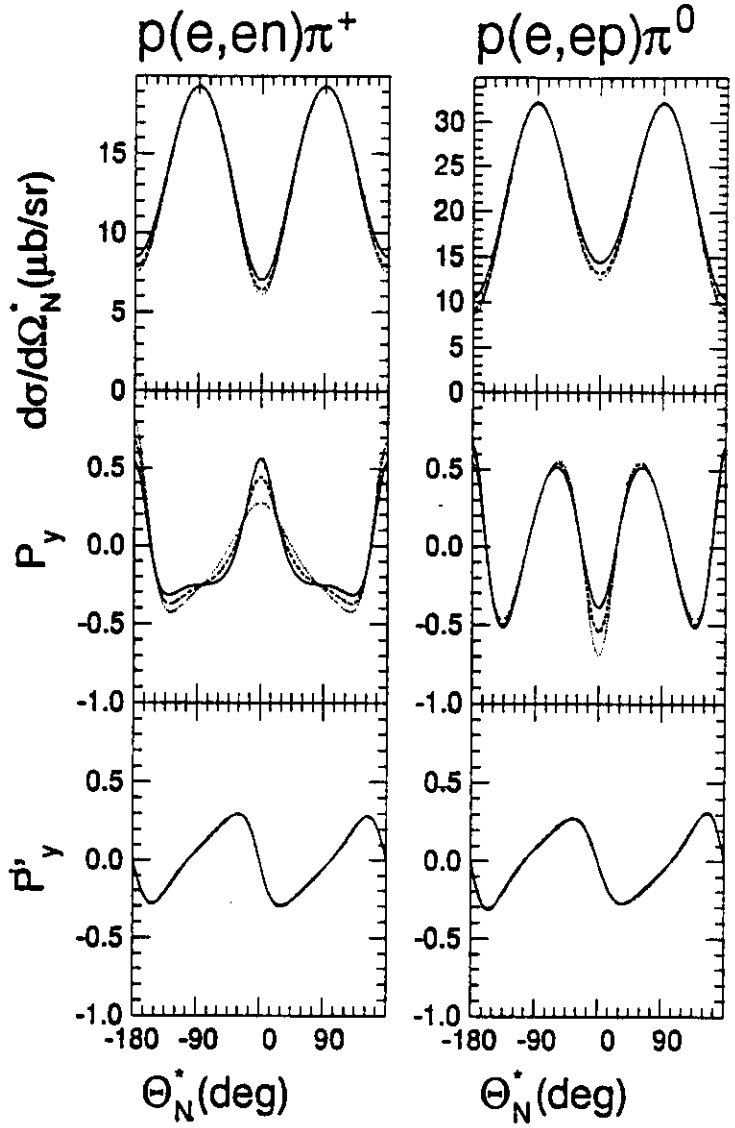


Figure 13: Observables for $W = 1.232$ GeV, $Q^2 = 0.5$ (GeV/c)$^2$, and $\epsilon = 0.9$ are compared for the $p(\vec{e}, e'\vec{n})\pi^+$ and $p(\vec{e}, e'\vec{p})\pi^0$ reactions at the delta resonance. Center of mass cross sections and laboratory polarizations are plotted against center of mass angle. The converter is oriented in the vertical orientation ($\phi = \pm 90°$) with $\theta_{nq} = 0$. Dotted curves use the DLvG parameters, whereas dot-dashed (solid) curves omit (invert) the quadrupole deformation.

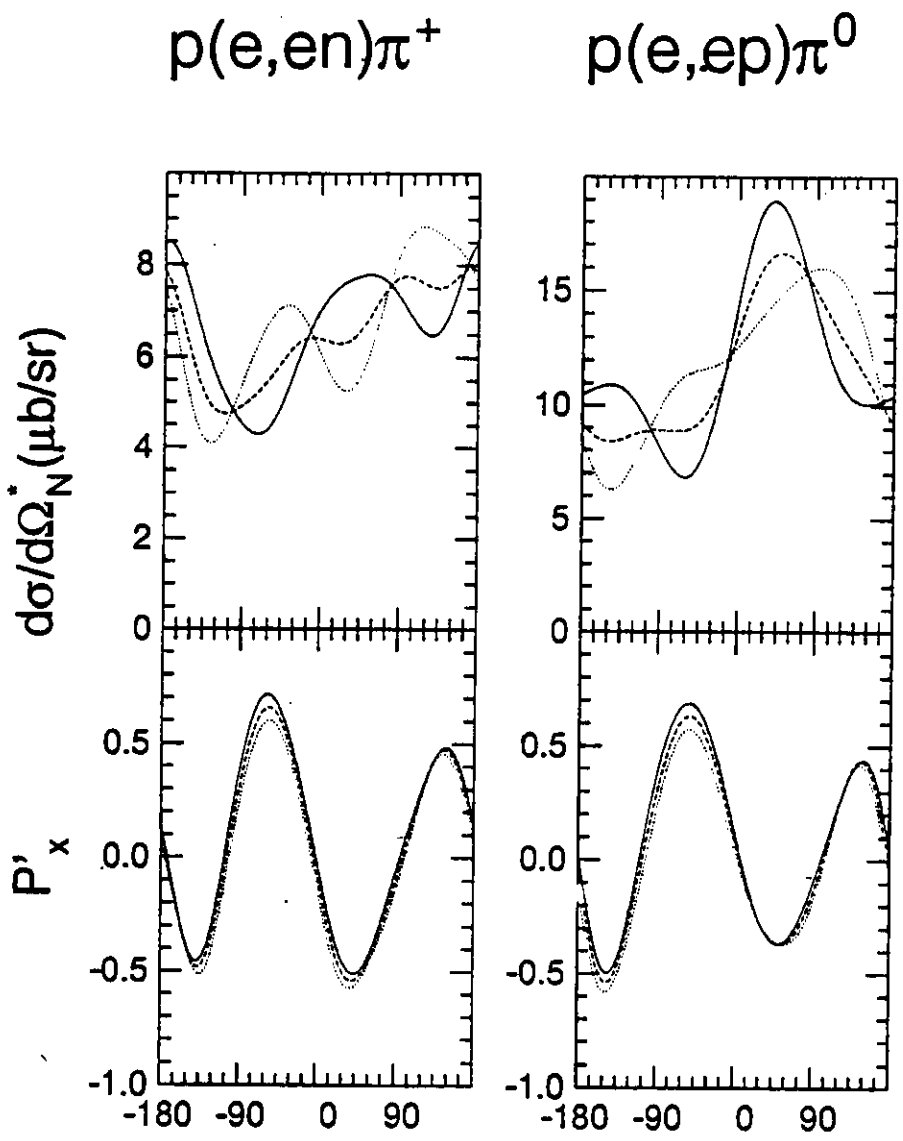


Figure 14: Observables for $W = 1.232$ GeV, $Q^2 = 0.5$ (GeV/c)$^2$, and $\epsilon = 0.9$ are compared for the $p(\vec{e}, e'\vec{n})\pi^+$ and $p(\vec{e}, e'\vec{p})\pi^0$ reactions at the delta resonance. Center of mass cross sections and laboratory polarizations are plotted against center of mass angle. The converter is oriented in the horizontal orientation ($\phi = 0$ or 180°) with $\theta_{nq} = 0$. Dotted curves use the DLvG parameters, whereas dot-dashed (solid) curves omit (invert) the quadrupole deformation.

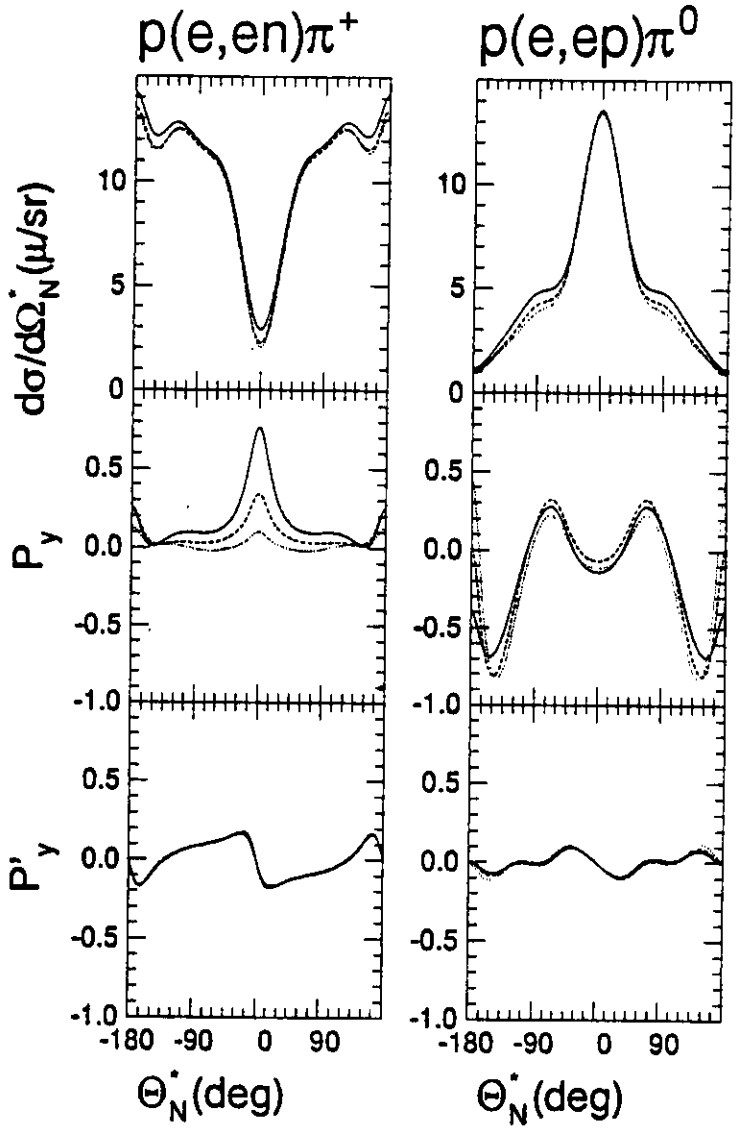


Figure 15: Observables for $W = 1.44$ GeV, $Q^2 = 0.23$ (GeV/c)$^2$, and $\epsilon = 0.9$ are compared for the $p(\vec{e}, e'\vec{n})\pi^+$ and $p(\vec{e}, e'\vec{p})\pi^0$ reactions at the Roper resonance. Center of mass cross sections and laboratory polarizations are plotted against center of mass angle. The converter is oriented in the vertical orientation ($\phi = \pm 90°$) with $\theta_{nq} = 0$. Dotted curves omit the Roper resonance, whereas dot-dashed (solid) curves use the hybrid (radial) models.

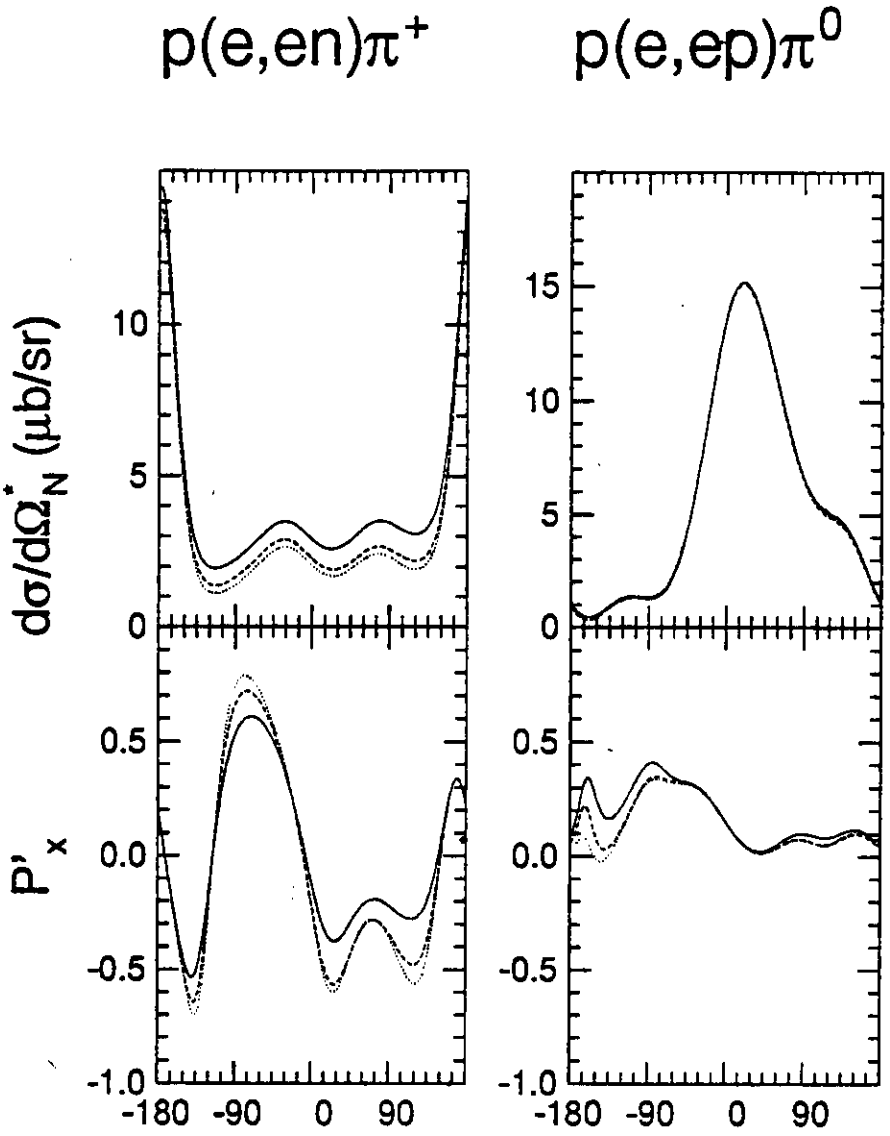


Figure 16: Observables for $W$ = 1.44 GeV, $Q^2$ = 0.23 (GeV/c)$^2$, and $\epsilon$ = 0.9 are compared for the $p(\vec{e}, e'\vec{n})\pi^+$ and $p(\vec{e}, e'\vec{p})\pi^0$ reactions at the Roper resonance. Center of mass cross sections and laboratory polarizations are plotted against center of mass angle. The converter is oriented in the horizontal orientation ($\phi$ = 0 or 180°) with $\theta_{nq}$ = 0. Dotted curves omit the Roper resonance, whereas dot-dashed (solid) curves use the hybrid (radial) models.

## 3.3 Count Rate Estimates

Count rate estimates for this experiment were based upon the parameters for the detectors that are listed in Table 2. In particular, we assume that a 13 cm liquid hydrogen target, with a thickness of about 1.0 g/cm$^2$ will be available. Furthermore, we assume that beam currents up to 100 $\mu$A will be available with greater than 60% polarization. Standard HRS1 parameters are employed.

The solid angle for HARP is determined by the converter dimensions and the distance. The minimum distance is constrained at small angles by the size of the HARP shielding enclosure. We plan to sort the data into square 3 x 3 cm$^2$ bins at the converter. For the $\Delta$ kinematics the converter distance of 0.8 m corresponds to solid angle bins of about 1.4 msr per bin, whereas at a distance of 1.6 m for the Roper distance the same bins correspond to about 0.35 msr per bin. Although these distances could be reduced slightly for larger $\theta_{nq}$, we plan to maintain fixed distances for each series of measurements to minimize variations of acceptance and efficiency. Approximately 25 bins per $\theta_{nq}$ setting will then span $\pm 180°$ for the $\Delta$ or $\pm 40°$ for the Roper resonance.

We used the DLvG model to estimate the laboratory cross sections for the proposed kinematics. These estimates are listed in Table 3. Since the cross sections are generally larger for $p(\vec{e}, e'\vec{p})\pi^0$ than for $p(\vec{e}, e'\vec{n})\pi^+$, the latter dictate the running times. Each laboratory opening angle $\theta$ corresponds to two center of mass angles $\theta^*_N$, where the forward branch has much higher kinetic energy than the backward branch. For the $\Delta$ kinematics, kinetic energies are in the range of about 300 - 440 MeV for the forward branch and 100 - 130 MeV for the backward branch. The two branches can be easily distinguished, but the cm $\rightarrow$ lab Jacobian strongly favors the forward branch (by about a factor of 5). At $Q^2 = 0.23$ (GeV/c)$^2$, the kinetic energies for the backward branch of the Roper distribution fall below the HARP detection threshold. In both cases, the laboratory cross sections for the two branches do not vary rapidly with angle (except near the turning point or rainbow), and are smallest for parallel kinematics. Therefore, we base the beam time request on the cross section for parallel kinematics and accept reduced statistics for very large $\theta^*_N$.

## 3.4 Beam Time Request

If $\alpha = (N_+ - N_-)/(N_+ + N_-)$ is the asymmetry within the polarimeter, the number of counts needed to reach a statistical precision of $\delta R/R$ in a generic polarized response function of the form $R \propto \sigma\Pi$ requires a total of

$$N \sim \left(\frac{R}{\alpha \delta R}\right)^2$$

counts. If $\Pi$ is the incident polarization and $\bar{A}$ is the effective analyzing power of the polarimeter, the asymmetry becomes $\alpha = \Pi\bar{A}$. Assuming that $\bar{A} \sim 0.25$ and $\Pi \sim 0.1$, a 10% measurement of $R$ would require $N \sim 1.6 \times 10^5$ counts. Therefore, a reasonable goal would be approximately $10^5$ counts per bin.

Table 2: *Experimental Parameters*

| | | |
|---|---|---|
| beam current | 100 $\mu$A | |
| target thickness | 1.0 g/cm$^2$ | |
| beam polarization | 0.6 | |
| HRS1 acceptance | 8 msr | |
| HRS1 momentum bite | 10% | |
| HARP efficiency | 0.01 | |
| HARP converter dimensions | 3 cm x 80 cm | |
| HARP bin size | 3 cm x 3 cm | |
| HARP distance | 0.8 m | 1.6 m |
| HARP solid angle | 1.40 msr | 0.35 msr |

Table 3: *Count Rate Estimates for Parallel Kinematics*

| W GeV | $Q^2$ (GeV/c)$^2$ | $\epsilon$ | $\sigma(e,e'n)\pi^+$ nb/GeV/sr$^2$ | rate hr$^{-1}$ | hours/ ($10^5$ counts) |
|---|---|---|---|---|---|
| 1.232 | 0.5 | 0.9 | 224.5 | $5.9 \times 10^3$ | 17 |
| 1.44 | 0.23 | 0.9 | 143.7 | $9.0 \times 10^2$ | 111 |

Estimated times for reaching $10^5$ counts for various kinematic conditions are listed in Tables 3. Approximately 24 hours of beam time are needed to attain the desired statistics in each angular bin for each of the six HARP settings at the $\Delta$ resonance, for a total of 144 hours. Similarly, approximately 112 hours per setting at the Roper resonance requires 672 hours. We assume that approximately 24 hours will be required for each of two transitions between horizontal and vertical configurations and that about 4 hours will be needed for each change of the HARP angle, for a total overhead of 96 hours. Finally, we ask for three days of set-up and calibration time. Therefore, we request a total of 984 hours of beam time. Details of the request are given in Table 4.

Table 4: *Beam Time Request*

| W (GeV) | $Q^2$ (GeV/c)$^2$ | $\theta_{nq}$ (deg) | mode | hours |
|---|---|---|---|---|
| 1.232 | 0.5 | 0 | horizontal | 24 |
| | | 0 | vertical | 24 |
| | | 4 | vertical | 24 |
| | | 8 | vertical | 24 |
| | | 12 | vertical | 24 |
| | | 16 | vertical | 24 |
| | | | subtotal | 144 |
| 1.44 | 0.23 | 0 | horizontal | 112 |
| | | 0 | vertical | 112 |
| | | 3.6 | vertical | 112 |
| | | 7.2 | vertical | 112 |
| | | 10.8 | vertical | 112 |
| | | 14.4 | vertical | 112 |
| | | | subtotal | 672 |
| | | | data | 816 |
| | | | overhead | 96 |
| | | | set-up | 72 |
| | | | total | 984 |

# Appendix A Observables and Response Functions

The kinematics for pion electroproduction are illustrated in Fig. 17. The angle between the leptonic scattering plane (containing the initial and final electron 3-vectors) and the hadronic reaction plane (containing the 3-momentum transfer q and the final nucleon 3-momentum $\mathbf{p}_{N_f}$) is denoted by $\phi_N = \phi_\pi - 180°$. The angles between the 3-momentum transfer and the laboratory momenta of final nucleon momentum and the pion are denoted by $\theta_N$ and $\theta_\pi$, respectively. Note that for $\phi_N = 0°$ and $\theta_N > 0°$, the nucleon recoils at a more forward angle than the 3-momentum transfer. The hadronic center of momentum frame is defined by the condition $\mathbf{q}^* + \mathbf{p}^*_{N_i} = \mathbf{p}^*_{N_f} + \mathbf{p}^*_\pi = 0$. The response functions can be considered functions of the invariant quantities

$$Q^2 = -q^2 = -(k_i - k_f)^2 = 2k_i k_f \sin^2(\theta_e/2)$$

$$W = \sqrt{s} = \sqrt{(q^* + p^*_{N_i})^2} = \sqrt{(p^*_\pi + p^*_{N_f})^2} = E^*_\pi + E^*_{N_f}$$

and the c. m. recoil nucleon angle $\theta^*_N = 180° - \theta^*_\pi$.

The recoil polarization is usually measured with respect to the helicity frame defined by the basis vectors

$$\begin{aligned} \hat{\mathbf{l}} &= \frac{\mathbf{p}^*_N}{|\mathbf{p}^*_N|} \\ \hat{\mathbf{n}} &= \frac{\mathbf{q}^* \times \hat{\mathbf{l}}}{|\mathbf{q}^* \times \hat{\mathbf{l}}|} \\ \hat{\mathbf{t}} &= \hat{\mathbf{n}} \times \hat{\mathbf{l}}. \end{aligned}$$

This basis is well defined when $\theta^*_N$ is not equal to 0° or 180°, but difficulties arise when $\mathbf{q}^*$ and $\mathbf{p}^*_N$ are either parallel or antiparallel and $\phi_N$ loses physical meaning. These cases are conventionally handled by first rotating the reaction plane to $\tilde{\phi}_N$ as it would be in non-parallel kinematics, and then taking the limit $\theta^*_N \to 0°$ or $\theta^*_N \to 180°$ as required.

The electroproduction cross section can be expressed in the form

$$\frac{d\sigma}{d\omega d\Omega_e d\Omega^*_N} = \frac{1}{2}\sigma_0 \left[1 + \vec{P} \cdot \vec{\sigma} + h(A + \vec{P}' \cdot \vec{\sigma})\right] \qquad \text{(A.1)}$$

where $\sigma_0 = K\tilde{\sigma}_0$ is the unpolarized cross section, $\vec{P}$ is the induced-polarization coefficient, $A$ is the beam analyzing power, $\vec{P}'$ is the polarization-transfer coefficient, $h$ is the electron helicity, and $\vec{\sigma}$ is the nucleon polarization vector. Thus, the net polarization of the recoil nucleon $\vec{\Pi}$ has two contributions of the form

$$\vec{\Pi} = \vec{P} + h\vec{P}'. \qquad \text{(A.2)}$$

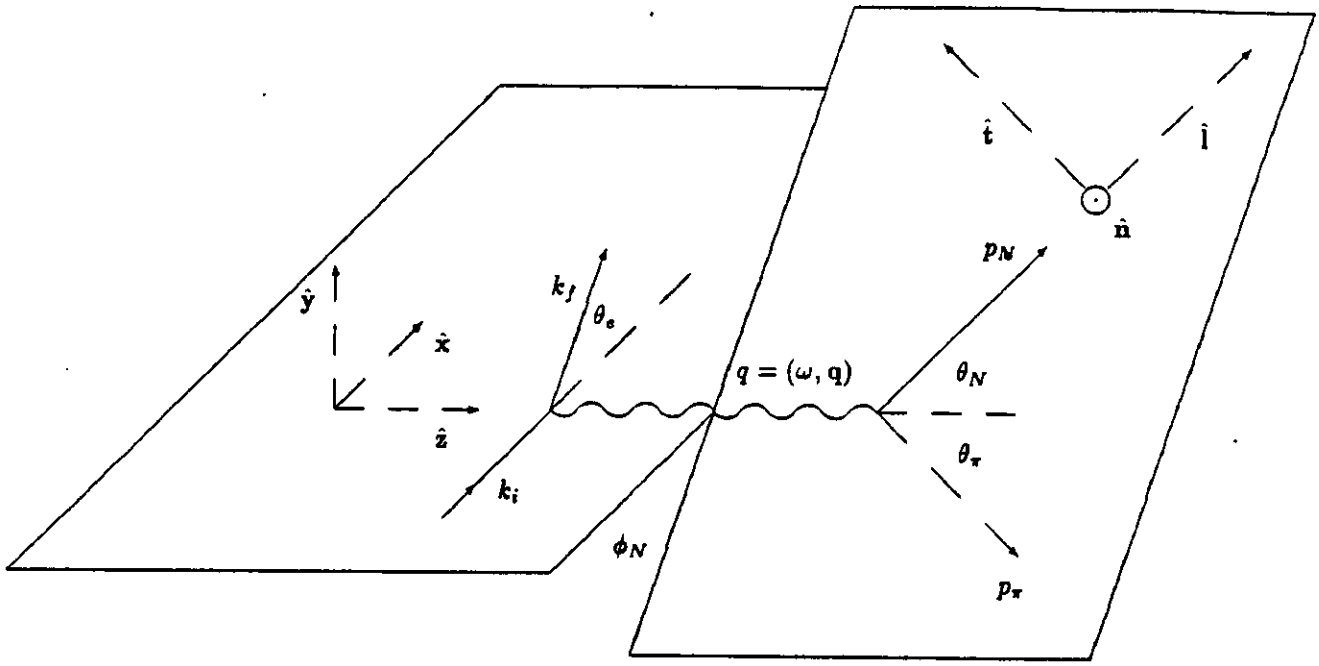


Figure 17: Kinematics for pion production. $k, k'$ represent initial and final electron 4-vectors, $q$ the 4-momentum transfer, $p_\pi$ the pion and $p_N$ the nucleon 4-momenta.

It is customary to express the differential cross section in terms of laboratory quantities for the electron and center-of-mass quantities for the hadrons, such that

$$\sigma_0 = K\tilde{\sigma}_0 = K^*\tilde{\sigma}_0\frac{d\Omega_N^*}{d\Omega_N} \tag{A.3}$$

where

$$K^* = \frac{p^*W}{k_\gamma m_p}\Gamma_\gamma \tag{A.4}$$

is a phase-space factor,

$$\Gamma_\gamma = \frac{\alpha}{2\pi^2}\frac{k_f}{k_i}\frac{k_\gamma}{Q^2}\frac{1}{1-\epsilon} \tag{A.5}$$

is the virtual photon flux,

$$\epsilon = \left(1 + 2\frac{|\mathbf{q}|^2}{Q^2}\tan^2\frac{\theta_e}{2}\right)^{-1} \tag{A.6}$$

is the virtual photon polarization, and

$$\epsilon_L = \frac{Q^2}{(\omega^*)^2}\epsilon \tag{A.7}$$

is the virtual photon longitudinal polarization. The quantity

$$k_\gamma = \frac{W^2 - m_p^2}{2m_p} \tag{A.8}$$

can be interpreted as the energy a real photon would need to excite the same transition.

Regrettably, no accepted standard for the signs and normalizations of the response functions has gained wide acceptance. We have chosen a convention for which all of the response functions enter the formulas with positive signs and all of the kinematical factors are also positive. Finally, we have evaluated the longitudinal polarization of the virtual photon in the c.m. frame.

The unpolarized cross section can be expressed in terms of four response functions

$$\tilde{\sigma}_0 = \nu_L R_L + \nu_T R_T + \nu_{LT} R_{LT} \cos\phi + \nu_{TT} R_{TT} \cos 2\phi \tag{A.9}$$

where $R_L$ is the longitudinal, $R_T$ the transverse, $R_{LT}$ the longitudinal-transverse interference, and $R_{TT}$ the transverse-transverse interference response function and where

$$\nu_L = 2\epsilon_L \tag{A.10}$$

$$\nu_T = 1 \tag{A.11}$$

$$\nu_{LT} = [\epsilon_L(1+\epsilon)]^{\frac{1}{2}} \tag{A.12}$$

$$\nu_{TT} = \epsilon \tag{A.13}$$

are kinematic coupling factors which depend only upon the lepton variables. Similarly, the induced polarization can be expressed in terms of response functions which depend upon the orientation of the polarization of the recoil nucleon as follows:

$$\tilde{\sigma}_0 P_n = \nu_{LT} R^n_{LT} \cos\phi + \nu_{TT} R^n_{TT} \cos 2\phi + \nu_L R^n_L + \nu_T R^n_T \tag{A.14}$$

$$\tilde{\sigma}_0 P_l = \nu_{LT} R^l_{LT} \sin\phi + \nu_{TT} R^l_{TT} \sin 2\phi \tag{A.15}$$

$$\tilde{\sigma}_0 P_t = \nu_{LT} R^t_{LT} \sin\phi + \nu_{TT} R^t_{TT} \sin 2\phi. \tag{A.16}$$

Finally, the observables which depend upon the electron helicity are expressed in terms of response functions whose dependence upon helicity is indicated by primes as follows:

$$\tilde{\sigma}_0 A = \nu'_{LT} R'_{LT} \sin\phi \tag{A.17}$$

$$\tilde{\sigma}_0 P'_n = \nu'_{LT} R'^n_{LT} \sin\phi \tag{A.18}$$

$$\tilde{\sigma}_0 P'_l = \nu'_{LT} R'^l_{LT} \cos\phi + \nu'_{TT} R'^l_{TT} \tag{A.19}$$

$$\tilde{\sigma}_0 P'_t = \nu'_{LT} R'^t_{LT} \cos\phi + \nu'_{TT} R'^t_{TT} \tag{A.20}$$

where

$$\nu'_{LT} = [\epsilon_L(1-\epsilon)]^{\frac{1}{2}} \tag{A.21}$$

$$\nu'_{TT} = \left[1-\epsilon^2\right]^{\frac{1}{2}}. \tag{A.22}$$

Considerable simplification of the spin structure of the reaction is obtained for parallel kinematics because only two of the six possible helicity amplitudes survive. Hence, only four independent response functions can contribute in parallel kinematics to pion electroproduction upon the nucleon. The expressions relating observables to response functions then reduce to

$$\tilde{\sigma}_0 = 2\epsilon_L R_L + R_T \quad \text{(A.23)}$$

$$\tilde{\sigma}_0 \Pi_n = \nu_{LT} R^n_{LT} \quad \text{(A.24)}$$

$$\tilde{\sigma}_0 \Pi_t = h\nu'_{LT} R'^t_{LT} \quad \text{(A.25)}$$

$$\tilde{\sigma}_0 \Pi_l = h\nu'_{TT} R'^l_{TT} \quad \text{(A.26)}$$

where the symmetries of one-photon exchange require $R'^l_{TT} = R_T$ in parallel kinematics. Azimuthal symmetry around $\mathbf{q}$ also requires $R^n_{LT} = R^t_{LT}$ and $R'^n_{LT} = -R'^t_{LT}$ in parallel kinematics. Thus, polarization measurements permit certain individual response functions to be isolated. Measurement of the induced polarization $P_n$ for parallel kinematics yields $R^n_{LT}(W, Q^2, \theta^*_N)$ at $\theta^*_N = 0°$ or $180°$ directly, whereas measurement of $P'_t$ yields $R'^t_{LT}$. Furthermore, for parallel kinematics it is not necessary to determine the longitudinal polarization since $R'^l_{TT} = R_T$. Therefore, measurements of the transverse polarization combined with Rosenbluth separation of the cross section suffice to completely determine the two relevant helicity amplitudes. Also note that different helicity amplitudes are obtained for $\theta^*_N = 0°$ and $\theta^*_N = 180°$.

# References


[1] R.W. Lourie. Recoil Polarization Observables in Coincident Pion Electroproduction. *Nucl. Phys.*, **A509**:653–663, 1990.

[2] R.W. Lourie. Quark Models and Polarized Electroproduction of the Roper Resonance. *Zeit. Phys.* C, **50**:345–351, 1991.

[3] D. Drechsel and L. Tiator. Threshold Pion Photoproduction on Nucleons. *J. Phys. G*, **18**:449–497, 1992.

[4] C.N. Papanicolas. Experimental Status of the $N \rightarrow \Delta$ Transition. In G. Adams, N.C. Mukhopadhyay, and P. Stoler, editors, *Excited Baryons 1988*, pages 235–255. World Scientific, Singapore, 1989.

[5] V. Burkert. Electroproduction of Light Quark Baryons. In H.P. Blok, J.H. Koch, and H. de Vries, editors, *Electromagnetic Production of Mesons on Nucleons and Nuclei.* NIKHEF, Amsterdam, 1992.

[6] Z. Li, V. Burkert, and Z. Li. Electroproduction of the Roper Resonance as a Hybrid State. CEBAF preprint PR-91-032, 1991.

[7] T.M. Payerle. User Manual for *EPIPROD* . unpublished, 1993.

[8] R.C.E. Devenish and D.H. Lyth. A Dispersion Relation Calculation of Neutral $\pi$ Meson Electroproduction in the Resonance Region. *Nucl. Phys.*, **B43**:228–252, 1972.

[9] R.C.E. Devenish and D.H. Lyth. Single $\pi^+$ Electroproduction at $w \approx 2$ GeV and the Pion Form Factor. *Phys. Rev.* D, **5**:47–59, 1972.

[10] R.C.E. Devenish and D.H. Lyth. Fixed-t Dispersion Approach and Single Pion Photoproduction in the Resonance Region. *Nucl. Phys.*, **B59**:237–255, 1973.

[11] G. von Gehlen. Dispersion Relations for Electroproduction Partial-Wave Amplitudes. *Nucl. Phys.*, **B9**:17, 1969.

[12] K.M. Watson. Some General Relations between the Photoproduction and Scattering of $\pi$ Mesons. *Phys. Rev.*, **95**:228–236, 1954.

[13] S. Mehrotra and L.E. Wright. Pion Electroproduction in the Non-Relativistic Limit. *Nucl. Phys.*, **A362**:461–479, 1981.

[14] I. Blomqvist and J.M. Laget. *Nucl. Phys.*, **A280**:405, 1977.

[15] S. Nozawa, B. Blankleider, and T.S.H. Lee. A Dynamical Model of Pion Electroproduction on the Nucleon. *Nucl. Phys.*, **A513**:459–510, 1990.

[16] S. Nozawa, B. Blankleider, and T.S.H. Lee. Electroproduction of Pions on the Nucleon (I). *Nucl. Phys.*, **A513**:511–542, 1990.

[17] S. Nozawa, B. Blankleider, and T.S.H. Lee. Electroproduction of Pions on the Nucleon (II). Polarization Observables. *Nucl. Phys.*, **A513**:543–556, 1990.